Chapter 11
Experimental System Identification and Tower-Top Dynamic Response of Monopile-Supported Offshore Wind Turbines During Installation

Saravanan Bhaskaran, Max Kruse, Andrew Goupee and Amrit Verma

Abstract The upscaling of offshore wind turbines (OWTs) in pursuit of improved efficiency introduces new structural dynamics challenges during the installation phase due to large hub heights. The blade–hub mating process, in particular, demands high precision, and unpredictable tower-top motion during this phase can result in damage to blades or guide pins. This paper presents a scaled experimental study on the dynamic response of monopile-supported OWTs based on the International Energy Agency (IEA) 10 MW and 15 MW reference turbines fabricated at 1:70 Froude-scale. System identification tests were conducted for both models to extract modal parameters such as natural frequencies, damping ratios, mode shapes, and stiffness distributions. The tower-top motions of the 10 MW model were subsequently measured under regular waves in a controlled flume environment. This work provides benchmark data to support predictive modeling, digital twin development, and control strategies for future offshore wind turbine installations.

Keywords Offshore · Turbine · Dynamics · Modal · Installation

Introduction

Offshore wind energy is expanding worldwide as the demand for large-scale renewable power grows, leading to the deployment of increasingly larger turbines. Monopile-supported offshore wind turbines (OWTs) have become the predominant foundation solution for the deployment of wind energy infrastructure in shallow to intermediate water depths due to their structural simplicity and cost-effectiveness. The installation phase of OWTs presents significant engineering challenges distinct from their operational state, as the system experiences a variety of dynamic loads that include wind, wave, and installation-induced forces prior to commissioning. A fundamental barrier to the robust and safe deployment of OWTs lies in understanding and quantifying their dynamic response during installation. The blade–hub mating process represents one of the most critical junctures in the installation of OWTs, as it requires precise alignment under dynamic environmental conditions. At this stage, the monopile, tower and nacelle are already installed in the hammerhead configuration, while the blades are lifted to the hub height by a crane vessel for attachment. OWTs are known to exhibit complex elliptical orbits with rapidly changing directions at the tower top in the hammerhead configuration [1], which can lead to damage at the blade root or the guide pins. Such risks underscore the potential to compromise equipment integrity, jeopardize personnel safety, and disrupt project schedules, making it essential to thoroughly investigate and characterize these responses.

A practical and cost-effective approach to investigating the underlying physics of complex engineering systems is through carefully designed scaled model tests conducted under controlled laboratory conditions [2]. Several studies have investigated the dynamic behavior of monopile-supported offshore wind turbines during their design and operational phases, employing scaled laboratory experiments and numerical simulations to evaluate modal properties and soil–structure interaction [3, 4, 5, 6, 7, 8]. These works have provided valuable insights into the long-term performance of monopile foundations under combined environmental loading conditions, including the effects of scour, soil stiffness, and nonlinear vibrations in waves. However, the majority of these efforts have focused on fully operational turbines, where the structural configuration and

Saravanan Bhaskaran · Max Kruse · Andrew Goupee · Amrit Verma
Department of Mechanical Engineering, University of Maine, USA
e-mail: saravanan.bhaskaran@maine.edu; max.kruse@maine.edu; agoupe91@maine.edu; amrit.verma@maine.edu

© The Author(s), under exclusive license to River Publishers 2026

Kristin B. Zimmerman, PhD (eds.), *Topics in Modal Analysis & Parameter Identification in Structural Dynamics, 2026, Vol. 8*,
Conference Proceedings of the Society for Experimental Mechanics Series, https://doi.org/10.13052/rp-9788743814191

boundary conditions differ significantly from those encountered during installation. As a result, there remains a lack of experimentally validated data capturing the unique dynamic responses that occur in the hammerhead configuration during installation.

This paper presents an experimental study focused on the design and testing of fully flexible 1:70 scale models of the International Energy Agency (IEA) 10 MW [9] and 15 MW [10] reference turbines in the hammerhead configuration. The natural frequencies, damping ratios, mode shapes, and stiffness distributions of both models were derived through a series of free-decay tests, roving accelerometer modal tests, and pull-out tests. The experimental findings were compared with high-fidelity numerical predictions to validate the modeling assumptions and highlight the sensitivities critical to installation planning. The 10 MW model was later installed in a wave flume where tower top motions were recorded for various regular wave conditions.

Methodology

This study focuses on the design and experimental testing of fully flexible 1:70 Froude-scaled models of the IEA 10 MW and 15 MW reference turbines in the hammerhead configuration, developed to replicate the dynamic response characteristics of the corresponding full-scale systems. Firstly, the approach used to obtain the experimental models is illustrated in Fig. 1, which depicts the progression from the full-scale distributed springs numerical model (baseline) to the final fabricated experimental model.

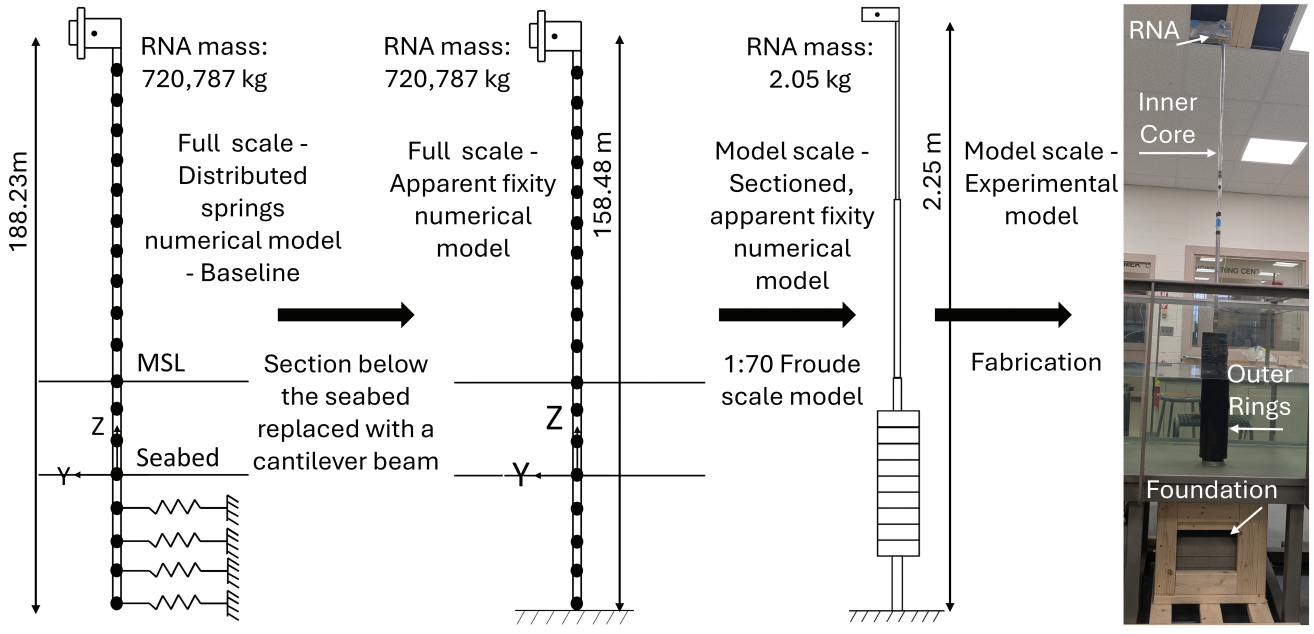

Fig. 1 Development of the 1:70 Froude-scale experimental model of the IEA 10 MW turbine

The numerical models used in this study were developed using the ASHES software package [11], a finite element analysis tool specifically designed for dynamic analyses of wind turbines. In the baseline representation, soil–structure interaction was modeled using a series of linear springs distributed along the embedded section of the monopile. Each node below the seabed was assigned three translational and three rotational stiffness constraints, with stiffness values calculated according to the equations provided in the IEA 15 MW turbine reference document [10]. The shear modulus of the soil was selected to represent dense sand conditions. The monopile and tower were modeled using Timoshenko beam elements, while the rotor–nacelle assembly (RNA) was represented as a lumped point mass with an eccentric offset relative to the tower axis. While the distributed springs model provides an accurate representation of the real soil–structure interaction, it is difficult to reproduce experimentally. Therefore, the apparent fixity method is adopted to simplify the soil representation by replacing the embedded section with an equivalent cantilever beam. The equivalent cantilever section below the seabed is required to produce the same deflection and rotation at the mudline as obtained from the baseline model. To achieve this, the 50-year return period load case was applied to the baseline model, assuming the turbine location along the U.S. East Coast near

New York. The resulting forces and bending moments were thereafter used to determine the equivalent bending stiffness and apparent fixity length, as described in [12]. The Froude scaling method was then used to reduce the structure to model-scale in order to preserve dynamic similarity between the model and the prototype. Froude scaling was chosen because wave–structure interactions are governed primarily by gravity, making the Froude number the controlling non-dimensional parameter. The primary Froude scaling relationships applied in this study are: length with λ, time with $\lambda^{0.5}$, mass and force with λ^3, and bending stiffness with λ^5, where λ is the scale factor. Since the full-scale structure features a varying diameter along its height, the model was divided into three uniform-diameter sections above the seabed and one section below the seabed to represent the embedded portion. The bending stiffness of the three sections above the seabed was averaged to match the overall stiffness distribution of the prototype, while the stiffness of the section below the seabed was accounted for using the apparent fixity method. The effectiveness of this sectioning approach in replicating the stiffness distribution of the prototype is shown in Fig. 2, where the modeled piecewise distribution of bending stiffness (EI) is compared with the baseline distributed springs representation for both turbines. This sectioning approach simplifies fabrication while retaining the essential dynamic fidelity of the prototype.

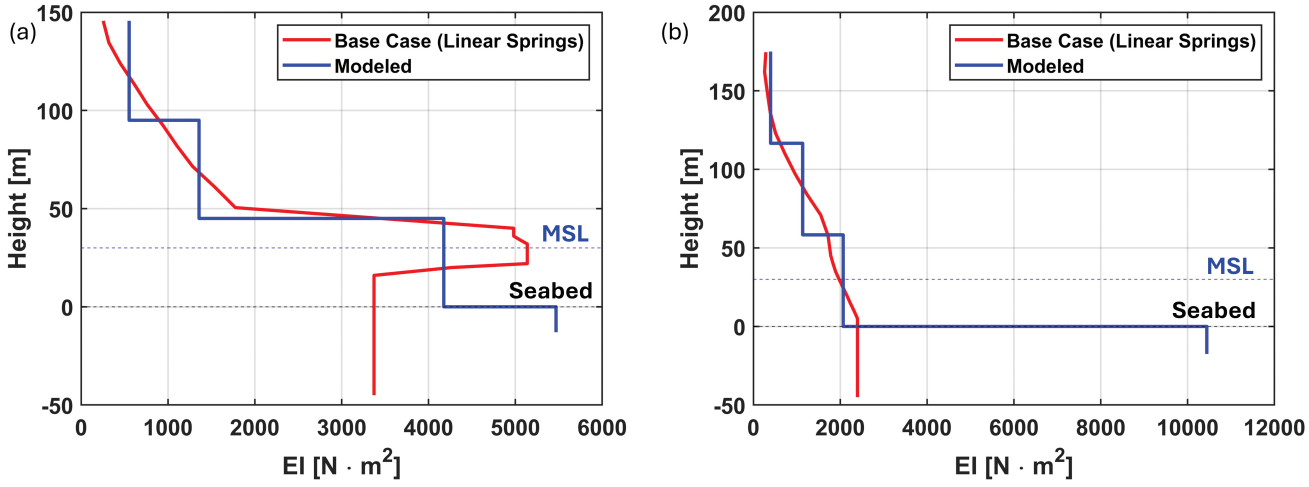

Fig. 2 Comparison of bending stiffness distributions: (a) IEA 10 MW (b) IEA 15 MW *Note: all values are reported in full-scale*

The experimental structure was assembled by welding four steel tube sections, each selected to achieve the required bending stiffness. An outer ring made of lightweight plastic was attached to the first section above the seabed to match the correct hydrodynamic diameter. The section below the seabed was clamped to a foundation containing heavy concrete slabs to enforce the fixed-end boundary condition at the base.

Results

System identification tests

Free decay tests

Free-decay tests were performed to identify the natural frequencies and damping ratios of the scaled turbine models. In these tests, the tower was excited using a rubber mallet, allowing the structure to oscillate freely. The resulting acceleration time histories were recorded with a piezoelectric accelerometer, and logarithmic decrement analysis was applied to estimate the damping ratios.

Two sets of modes were identified in both the fore–aft (FA) and side–side (SS) directions for the scaled turbine models. The corresponding natural frequencies and damping ratios for the 10 MW and 15 MW turbines are summarized in Tables 1 and 2, respectively. To align the first set of natural frequencies with the baseline model, the RNA mass was artificially increased by approximately 13% for the 10 MW model and 8% for the 15 MW model. This study focuses primarily on the first set of modes, as they are the most critical for capturing tower-top motions.

Table 1 Comparison of natural frequencies for the 10 MW turbine model

Mode	Baseline [Hz]	Modeled [Hz]	Experiment [Hz]	Damping [%]
Mode 1 (SS)	0.296	0.293	0.295	0.092
Mode 1 (FA)	0.297	0.294	0.297	0.175
Mode 2 (FA)	1.606	2.437	2.235	0.365
Mode 2 (SS)	1.622	2.498	2.309	0.316

Table 2 Comparison of natural frequencies for the 15 MW turbine model

Mode	Baseline [Hz]	Modeled [Hz]	Experiment [Hz]	Damping [%]
Mode 1 (SS)	0.185	0.185	0.185	0.279
Mode 1 (FA)	0.185	0.185	0.185	0.308
Mode 2 (FA)	1.182	1.604	1.548	0.244
Mode 2 (SS)	1.208	1.633	1.582	0.229

Mode shapes

Mode shapes for both turbine models were obtained using roving accelerometer tests. An impulse force hammer was used to excite the tower at both hub height and mid-height in order to capture the first and second sets of modes. Measurements were taken at 18 elevations along the tower height in both the fore–aft and side–side directions. The acceleration time histories and the impact forces were recorded for each case. Frequency response functions (FRFs) were computed, and the modal displacements were normalized with respect to the maximum value. Multiple hammer strikes were performed at each sensor location to account for variability in the manual excitation. To ensure consistency, only normalized displacements that deviated by less than 5% from the baseline results were retained for analysis. Out of the eight mode shapes extracted, two representative cases are shown in Fig. 3, and these exhibit good agreement with the baseline results, indicating that the scaled models capture the dynamic behavior of the prototypes.

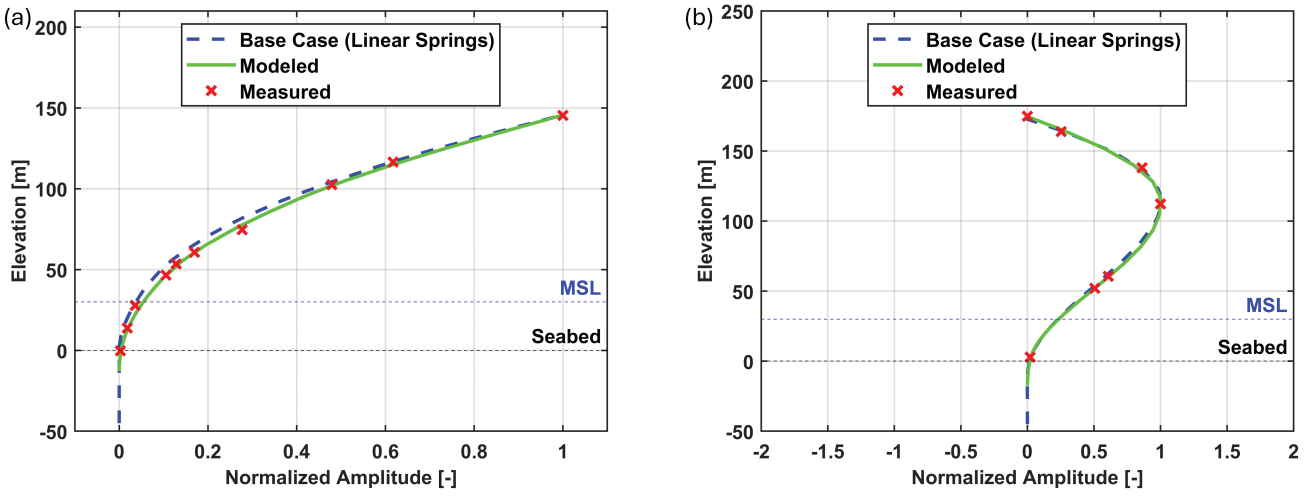

Fig. 3 Representative mode shapes (a) 10 MW 1st SS mode (b) 15 MW 2nd FA mode *Note: all values are reported in full-scale*

Pull-out tests

The stiffness of the physical models was evaluated through pull-out tests. Six measurement points were marked along the elevation of the tower, and varying known weights were applied near the tower top using a string and pulley arrangement to simulate static horizontal loading. The resulting displacements were measured with a high-speed camera. A reference image with a ruler was used to establish a pixel-to-millimeter conversion ratio, and the displacement of each marked point was determined by comparing images taken before and after the application of the loads. Tests were performed in all four

directions by rotating the foundation 90° for each iteration. Stiffness was calculated as the ratio of applied force to measured displacement, and the inverse (flexibility) was also derived, as shown in Fig. 4.

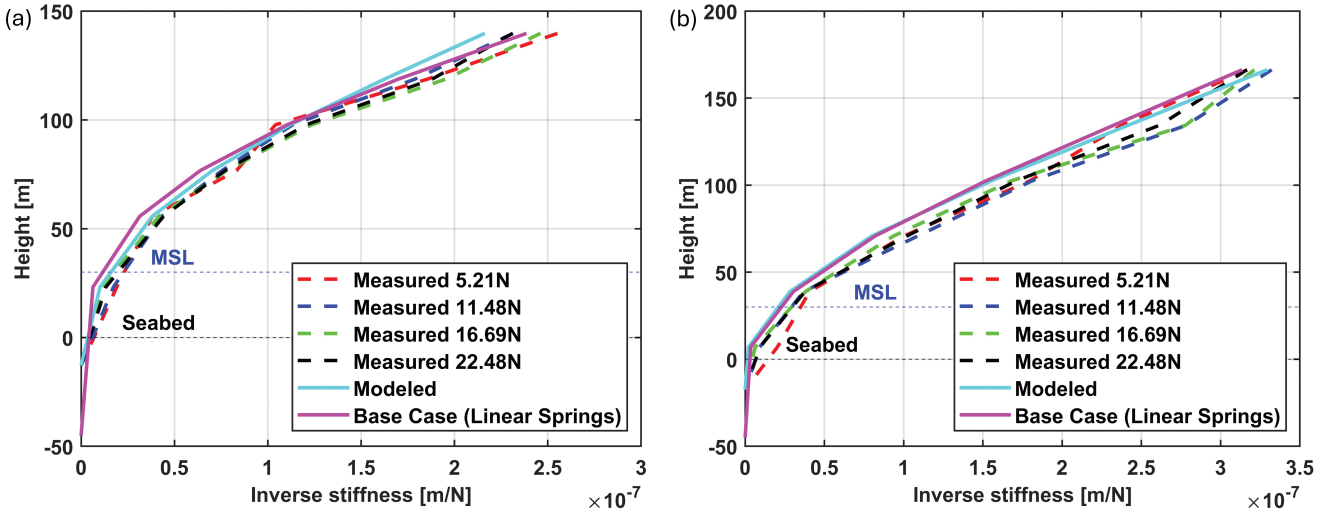

Fig. 4 Inverse stiffness distributions (a) 10 MW -X direction (b) 15 MW +X direction *Note: all values are reported in full-scale*

The results indicate strong linearity in stiffness and good agreement between the baseline and experimental observations.

Tower top motions

The 10 MW model was installed in a 10 m long wave flume to characterize its tower-top motion response under regular wave conditions. Two single-axis accelerometers were mounted on the nacelle to record motions in the X and Y directions at the tower-top. The tests were conducted at a model-scale wave height of 30 mm with periods of 0.4 s and 0.5 s, and an incident wave angle of 45°. Each load case was repeated six times, resulting in a total of 12 motion recordings. Each recording was approximately 1.25 minutes in duration, corresponding to about 10 minutes at full-scale. The recorded acceleration time histories were subsequently integrated twice, with appropriate filtering, to obtain the tower-top displacement trajectories in both the X and Y directions. Figure 5a illustrates the two-dimensional (2D) motion path at the tower top for a resonance case,

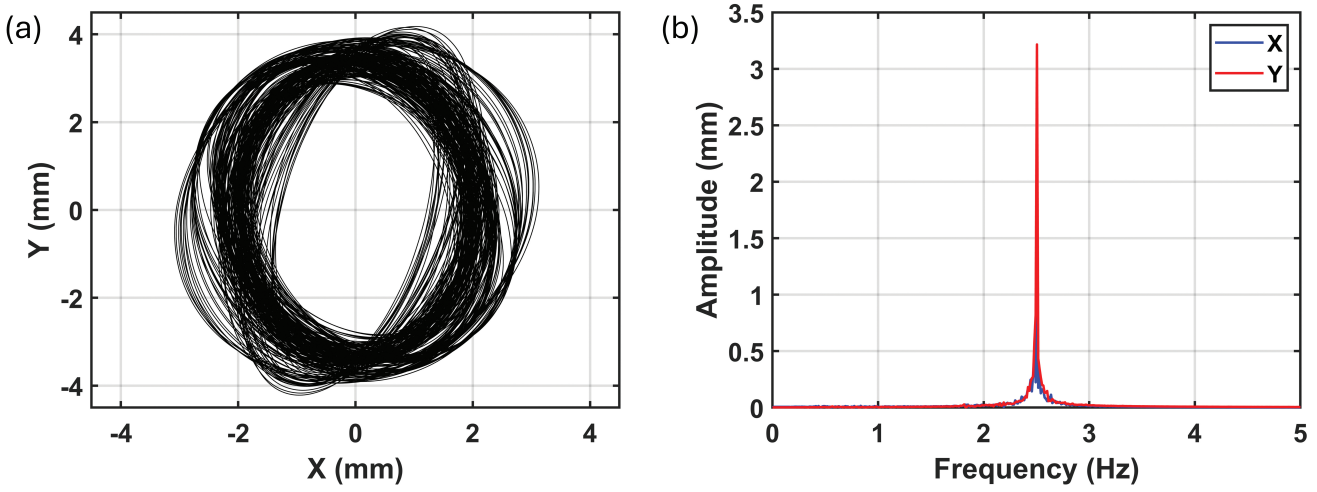

Fig. 5 (a) 2D motion path at the tower-top for H = 30 mm, T = 0.4 s θ_{wv} = 45° (b) frequency-domain response *Note: all values are reported in model-scale*

where the wave period of 0.4 s is close to the fundamental natural period of the system. In the frequency-domain response (Fig. 5b), a single sharp peak is observed at the resonant frequency of approximately 2.5 Hz. The time-domain trajectory reveals pronounced elliptical orbits that continuously change orientation. Such motions present significant challenges during the blade–hub mating phase, as the instability and rapid variation in orbital direction can hinder precise alignment.

Figure 6a shows the 2D motion trajectory at the tower top for the non-resonant case with a wave period of 0.5 s. The motion amplitude is significantly smaller compared to the resonant case, and the orbit remains consistently aligned with the incident wave angle of 45°. In the frequency-domain response (Fig. 6b), the dominant peak corresponds to the wave frequency of 2 Hz, accompanied by a smaller peak at the structural resonant frequency. Two additional secondary peaks are observed near the wave frequency, which result from reflected waves interacting to form a standing wave with a frequency offset of approximately 0.11 Hz. Minor noise contributions from the accelerometers are also visible, particularly due to the small displacement amplitudes.

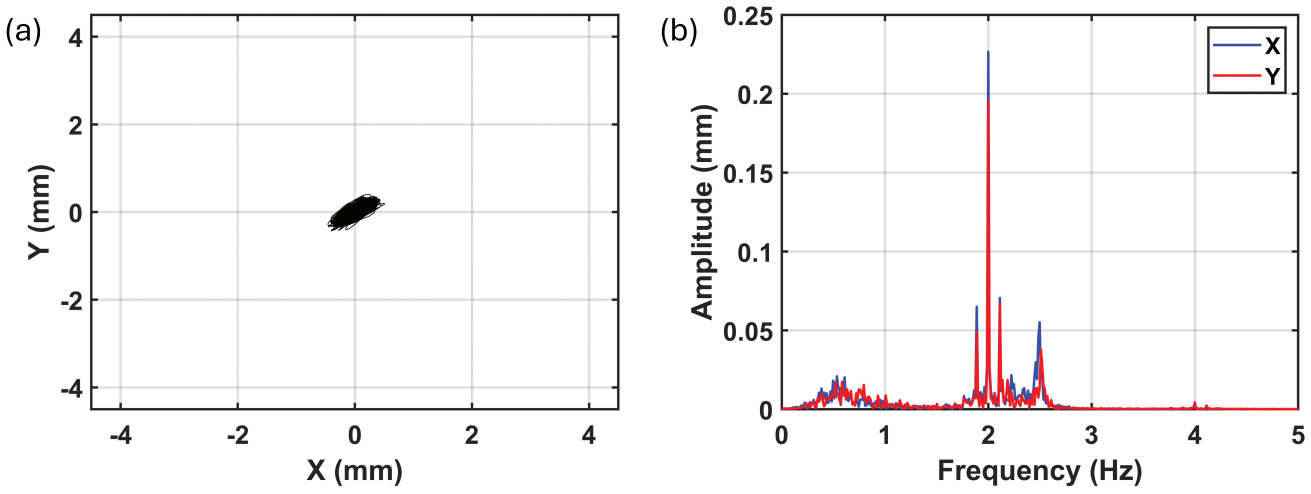

Fig. 6 (a) 2D motion path at the tower-top for H = 30 mm, T = 0.5 s $\theta_{wv} = 45°$ case (b) frequency-domain response *Note: all values are reported in model-scale*

Conclusions

This study presented fully flexible 1:70 scale models of the IEA 10 MW and 15 MW turbines in the hammerhead configuration, with system identification tests showing close agreement with numerical predictions of key dynamic properties. These results confirm the validity of the modeling approach and the suitability of the scaled structures for dynamic investigations. Tower-top motions of the 10 MW model were further characterized under regular wave forcing in a controlled wave flume. Resonant excitation produced complex elliptical orbital motions with rapidly changing orientations, while non-resonant conditions yielded small, stable orbits aligned with the wave direction. Such results highlight the dynamic instabilities that can occur during the blade–hub mating phase and underscore the importance of accounting for tower-top orbital motions in installation planning. Overall, the findings provide benchmark experimental data and validated modeling strategies that can support predictive tools, digital twin development, and improved risk management practices for offshore wind turbine installation.

Acknowledgments This research is funded by the National Science Foundation (NSF) through the Division of Chemical, Bioengineering, Environmental and Transport Systems (CBET) under Grant No. 2343210.

References

1. A. Sander, A. F. Haselsteiner, K. Barat, M. Janssen, S. Oelker, J.-H. Ohlendorf, and K.-D. Thoben, "Relative motion during single blade installation: Measurements from the north sea," in *International Conference on Offshore Mechanics and Arctic Engineering*, vol. 84416, p. V009T09A069, American Society of Mechanical Engineers, 2020.

2. S. Bhattacharya, G. Nikitas, and S. Jalbi, "On the use of scaled model tests for analysis and design of offshore wind turbines," in *Geotechnics for Natural and Engineered Sustainable Technologies: GeoNEst*, pp. 107–129, Springer, 2018.
3. L. Kerner, J.-C. Dupla, G. Cumunel, P. Argoul, J. Canou, and J.-M. Pereira, "Experimental study on a scaled model of offshore wind turbine on monopile foundation," in *Models, Simulation, and Experimental Issues in Structural Mechanics*, pp. 249–267, Springer, 2017.
4. R. Mayall, R. McAdam, B. Byrne, H. Burd, B. Sheil, P. Cassie, and R. Whitehouse, "Experimental modelling of the effects of scour on offshore wind turbine monopile foundations," in *Physical Modelling in Geotechnics, Volume 1*, pp. 726–730, CRC Press, 2018.
5. A. Buljac, H. Kozmar, W. Yang, and A. Kareem, "Concurrent wind, wave and current loads on a monopile-supported offshore wind turbine," *Engineering structures*, vol. 255, p. 113950, 2022.
6. S. Tian, C. Zhang, and Z. Wang, "Experimental study on the dynamic response of monopile supported offshore wind turbines in sand," *Ocean Engineering*, vol. 326, p. 120913, 2025.
7. S. Wu, H. Zhang, Z. Chen, X. Liu, L. Zheng, M. Du, R. Li, and D. Li, "Experimental study on nonlinear vibrations of flexible monopile-foundation offshore wind turbines in regular waves," *Water*, vol. 17, no. 8, p. 1176, 2025.
8. E. E. Bachynski, M. Thys, and F. Dadmarzi, "Observations from hydrodynamic testing of a flexible, large-diameter monopile in irregular waves," in *Journal of Physics: Conference Series*, vol. 1669, p. 012028, IOP Publishing, 2020.
9. P. Bortolotti, H. C. Tarres, K. Dykes, K. Merz, L. Sethuraman, D. Verelst, and F. Zahle, "Iea wind tcp task 37: Systems engineering in wind energy-wp2. 1 reference wind turbines," 2019.
10. E. Gaertner, J. Rinker, L. Sethuraman, F. Zahle, B. Anderson, G. Barter, N. Abbas, F. Meng, P. Bortolotti, W. Skrzypinski, *et al.*, "Definition of the iea 15-megawatt offshore reference wind turbine," 2020.
11. L. Suja-Thauvin, P. Thomassen, and A. Simis, "Engineering features summary,"
12. E. Bush and L. Manuel, "Foundation models for offshore wind turbines," in *47th AIAA aerospace sciences meeting including the new horizons forum and aerospace exposition*, p. 1037, 2009.